Nanoscale

COMMUNICATION

Enhanced synergism of thermo-chemotherapy by combining highly efficient magnetic hyperthermia with magnetothermally-facilitated drug release†

Yang Qu,[a] Jianbo Li,*[a,b] Jie Ren,*[a,b] Junzhao Leng,[a] Chao Lin[c] and Donglu Shi[c,d]

Cite this: *Nanoscale*, 2014, **6**, 12408

Received 18th June 2014,
Accepted 31st August 2014

DOI: 10.1039/c4nr03384a

www.rsc.org/nanoscale

A magnetothermally-responsive nanocarrier was developed for efficient thermo-chemotherapy by combining efficient magnetic hyperthermia (MH) and magnetothermally-facilitated drug release. The effective magnetothermal-response contributed to high enhancement of tumor cell killing by an operating mechanism involving MH-facilitated cellular uptake and Heat Shock Protein over-expression.

In the recent decades, magnetic fluid hyperthermia (MFH) has become a promising tumor treatment by targeted heating of non-invasive alternating magnetic field (AMF).[1] Meanwhile, magnetic fluid can also be used as the contrast agent of magnetic resonance imaging (MRI),[2] magnetic drug targeting (MDT),[3] and multi-treatment by combining with radiotherapy or chemotherapy.[4,5] Particularly, recent advances in highly efficient MRI agents and magnetic fluids have found that a magnetic nanocluster (MNC), a closed packing structure of multiple MNPs, shows a higher spin–spin (T_2) relaxivity and a specific adsorption rate (SAR) than a hydrophilic single MNP.[6,7] Meanwhile, the MNC can be loaded with a hydrophobic drug simultaneously in the core of the magnetic composite nanocarrier by encapsulation of amphiphilic polymers for tumor multi-treatment. In addition, functional amphiphilic polymers can be modified with biospecific ligands, such as antibodies, to target cancer cells efficiently by combining with MDT.[8] Therefore, the magnetic composite nanocarrier with MNC provides opportunities for design and development of efficient thermo-chemotherapy.

However, the synergistic effect of hyperthermia and chemotherapy is complicated by the two distinctively different treatments.[9,10] Their synergism is significantly affected by their spatial–temporal synchronism and efficiency of hyperthermia.[11] Apparently, efficient hyperthermia and spatial synchronism of thermo-chemotherapy can be ensured by a magnetic composite nanocarrier with MNC. In order to enhance their temporal synchronism, recent advances on composite nanocarriers have developed different kinds of magnetic liposomes/polymersomes/microspheres to integrate MFH with chemotherapy.[12–17] Moreover, several stimuli-responsive nanocarriers can also be utilized to coordinate MFH and chemotherapy based on environmental changes, such as redox, pH, and temperature.[18–20] Among all stimuli-responsive drug deliveries, the thermosensitive nanocarrier shows a unique advantage to enhance temporal synchronism of thermo-chemotherapy by associating drug release with hyperthermia.[21,22] Therefore, such a thermosensitive composite nanocarrier is capable of spatial–temporal synchronism of hyperthermia and chemotherapy.[23,24] By a physical or biological target, the distribution of MNCs can be controlled for targeted magnetic hyperthermia (MH).[25,26] Under an AMF, the targeted MNCs can raise temperature of the tumor region rapidly and accumulate chemotherapeutic agents by triggering their release from thermosensitive nanocarriers.[27] Moreover, efficient hyperthermia has been known to be effective in the enhancement of drug cytotoxicity.[28,29] Therefore, the ideal strategy of thermo-chemotherapy is to incorporate MNCs, drugs, and amphiphilic thermosensitive polymers, in an integrated fashion into the magnetothermally-responsive nanocarriers (MTRNs). Optimum therapeutic effects can be achieved including high drug concentration, enhanced drug cytotoxicity, lowering recommended dosages, and further alleviating the side effects.

In this study, we present a straightforward assembly of MTRN for highly efficient thermo-chemotherapy. The thermosensitive amphiphilic polymer polylactide-*b*-poly(*N*-isopropyl-

[a]*Institute of Nano and Bio-Polymeric Materials, School of Materials Science and Engineering, Tongji University, Shanghai 201804, China. E-mail: renjie6598@163.com*

[b]*Key Laboratory of Advanced Civil Materials, Ministry of Education, School of Materials Science and Engineering, Tongji University, Shanghai 201804, China. E-mail: lijianbo@tongji.edu.cn*

[c]*Key Laboratory of Basic Research in Cardiology, Ministry of Education, Shanghai East Hospital, Institute for Biomedical Engineering and Nano Science, School of Medicine, Tongji University, Shanghai 200120, China*

[d]*Materials Science and Engineering Program, Department of Mechanical and Materials Engineering, College of Engineering and Applied Science, University of Cincinnati, Cincinnati, OH 45221-0072, USA*

†Electronic supplementary information (ESI) available. See DOI: 10.1039/c4nr03384a

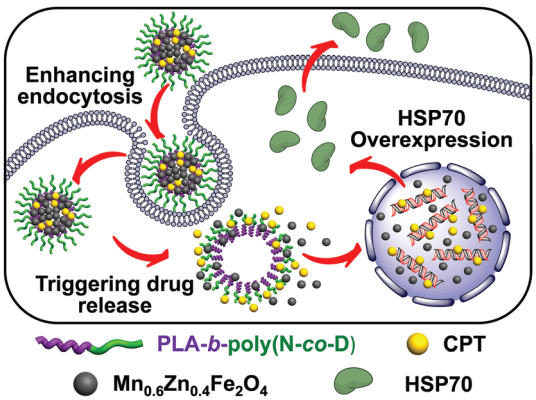

Scheme 1 Schematic illustration of synergistic mechanism between efficient magnetic hyperthermia and chemotherapy by magnetothermally-responsive nanocarriers, including enhancement of endocytosis, triggering drug release, and up-regulation of HSP70 expression.

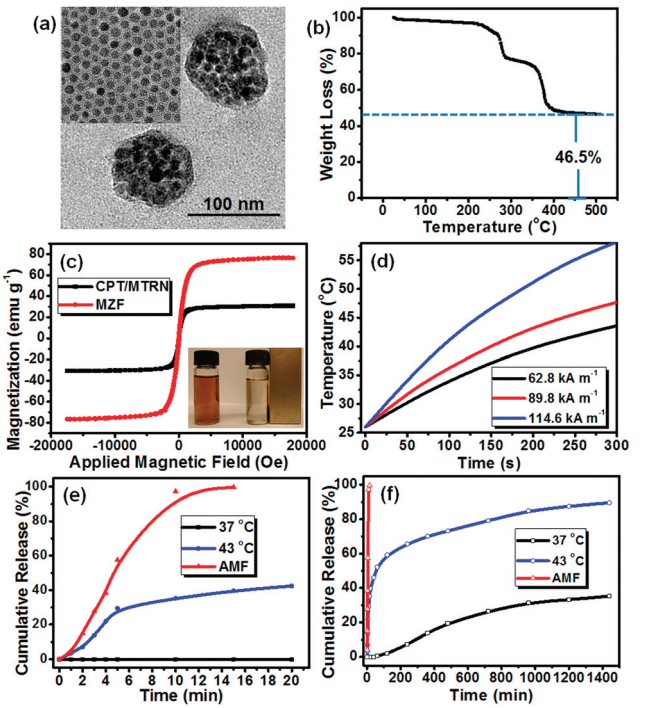

Fig. 1 (a) TEM image CPT/MTRNs; inset: TEM image of MZF; (b) TGA result of CPT/MTRNs; (c) magnetization curves of the MZF and CPT/MTRN at 300 K; inset: photograph of CPT/MTRN solution and its response to an external magnet; (d) time-dependent temperature curves of CPT/MTRNs in AMF (f = 114 kHz), (e) short-term drug release profiles of CPT/MTRNs (PBS, pH = 7.4) at 37 °C, 43 °C and AMF (f = 114, $H_{applied}$ = 89.9 kA m^{-1}); (f) long-term drug release profiles of CPT/MTRNs under the same conditions.

acrylamide-*co*-*N*,*N*-dimethylacrylamide) [PLA-*b*-poly(N-*co*-D)] was synthesized (Fig. S1†) and characterized (Fig. S2 and S3†). Its lower critical solution temperature (LCST) was adjusted at 42.5 °C (Fig. S4†), which is the optimal temperature for thermo-chemotherapy. By sonication, hydrophobic MNPs and chemotherapeutic drug camptothecin (CPT) were encapsulated simultaneously by PLA-*b*-poly(N-*co*-D) to develop the CPT-loaded MTRNs (CPT/MTRNs), in which the hydrophobic MNPs and CPT assemble spontaneously into tight nanoclusters. In theory, the magnetocaloric effect of MNCs is not only to trigger CPT release efficiently by AMF, but also to generate potential impacts on cellular responses to enhance CPT cytotoxicity, including enhancement of endocytosis and up-regulation of Heat Shock Protein 70 (HSP70) expression,[30,31] as shown in Scheme 1. Therefore, in further cell experiments we not only focused on significant synergistic effect of thermo-chemotherapy by CPT/MTRNs in AMF, but also tried to understand their synergistic mechanism.

The inset of Fig. 1a shows the transmission electron microscopy (TEM) image of the monodispersed hydrophobic MNPs ($Mn_{0.6}Zn_{0.4}Fe_2O_4$, MZF) with a narrow size distribution around 8 nm. The MZF was synthesized according to a method reported earlier,[32] and characterized by XRD shown in Fig. S5†. The CPT/MTRNs were developed by self-assembly with the feed ratio of PLA-*b*-poly(N-*co*-D), MZF and CPT as 45/45/10. As shown in Fig. 1a, the CPT/MTRNs exhibit spherical shapes around 100 nm with cores of MZF nanoclusters. Furthermore, the diameters of MZFs and CPT/MTRNs were indicated by DLS (Fig. S6†), coinciding with the TEM results. The CPT content was determined to be 9.9 wt% by UV-Vis (not shown). By thermogravimetric analysis (TGA, Fig. 1b), CPT/MTRN is shown to contain MZF of 46.5 wt%, which is close to its feed ratio.

The hysteresis loop profiles of MZF and CPT/MTRN exhibit superparamagnetism, shown in Fig. 1c. Therefore, CPT/MTRNs are well-distributed in phosphate buffered saline (PBS) without any precipitation for 24 h, shown in the inset of Fig. 1c. Moreover, the saturation magnetization (M_s) of MZF is 76.7 emu g^{-1}, which is considerably higher than that of Fe_3O_4.[33] Consequently, M_s of CPT/MTRN reached 30.8 emu g^{-1} for effective magnetic targeting. As also seen in the inset of Fig. 1c, the CPT/MTRNs of low concentration (200 μg mL^{-1}) show a good response to an external magnet.

The most important feature of CPT/MTRNs is to provide high SAR for triggering drug release and enhancing drug cytotoxicity. As shown in Fig. 1d, the heating profiles of CPT/MTRNs show that the MZF nanoclusters of low concentration (100 μg mL^{-1}) can raise the surrounding temperature rapidly under AMF. Even at the lowest strength of AMF ($H_{applied}$, 62.8 kA m^{-1}), the time required to raise the temperature from 26 °C to 42.5 °C by CPT/MTRNs is as short as 260 s, which is shorter than previous reports.[23,27,34] Based on the initial calefactive velocity of CPT/MTRNs, the max SAR is 1018.0 W g^{-1}, corresponding to the highest $H_{applied}$ of 114.9 kA m^{-1}. It is worth noting that SAR of CPT/MTRNs is multifold SAR values of other hydrophilic single MNPs (≤15 nm), in spite that M_s of the former is lower than those of the latter.[33,35–38] A similar behavior was reported by Xue *et al.*,[39] who found that $MnFe_2O_4$ nanoclusters decorated by graphene oxide can enhance their T_2 relaxivity value and SAR significantly. Comparing with graphene oxide, the advantages of thermosensitive nanocarriers

are not only to load magnetic nanoclusters and drug simultaneously, but also to associate drug release with efficient magnetic hyperthermia.

Due to high SAR of CPT/MTRNs, the CPT release is triggered efficiently by AMF, as shown in Fig. 1e. Based on the phase transition of a thermosensitive polymer, the amphiphilic polymer PLA-*b*-poly(N-*co*-D) will become the hydrophobic polymer abruptly at the temperature above its LCST, leading destruction of the micellar structure and aggregation of nanocarriers, as shown in Fig. S7†. Therefore, the CPT/MTRNs exhibit rapid CPT release triggered by AMF at 43 °C in 15 min because of their LCST at 42.5 °C. However, the drug release by AMF is much more pronounced compared to its counterpart at 43 °C. By AMF, the cumulative CPT release from CPT/MTRNs is 4.1% within 1 min, and reaching nearly 100% at 10 min. Such a rapid release upon AMF is facilitated by the MZF nanocluster of high SAR, which is combined with CPT directly in the core of the nanocarrier system. In addition, based on heating profiles shown in Fig. 1d, CPT/MTRNs with high SAR can raise the surrounding temperature from 37 °C to 44.1 °C within 1 min under AMF (f = 114 kHz, $H_{applied}$ = 89.9 kA m^{-1}). As a result, the CPT release takes place during the initial period. Moreover, the CPT/MTRNs can induce continuous temperature rise with increasing exposure time under AMF. Therefore, the system temperature induced by MH can be raised much higher than LCST of CPT/MTRNs and lead to an exponential increase of cumulative CPT release. In contrast, CPT/MTRNs exhibit considerable stability at 37 °C, as no CPT release is detected within 20 min.

The cumulative CPT release of prolonged time is also investigated, as shown in Fig. 1f. Apparently, CPT/MTRN displays temperature-dependent drug release. At 37 °C, the CPT release is hardly detected within 40 min. After that, CPT diffuses slowly from CPT/MRN and releases 35.2% within 24 h without trend of further release. At 43 °C, CPT/MTRN shows a continuous release behavior, as the cumulative release of CPT increases rapidly and reaches 59.3% within 120 min. Until 24 h, the cumulative release of CPT increases to 89.7%, which is 2.55 times of its counterpart by 37 °C. As the MZF nanocluster of high SAR can trigger CPT release efficiently from CPT/MTRN, cumulative CPT release reaches 100% within 15 min (Fig. 1e), which is much shorter than 24 h. Therefore, cumulative CPT release by AMF seems to reach 100% almost in an instant, as can be seen in Fig. 1f, showing a visual evidence for high efficiency of MH on triggering drug release.

Cytotoxicity experiments of CPT/MTRNs were carried out using SK-OV-3 (ovarian carcinoma cell line) and HepG2 (hepatocellular carcinoma cell line). Before evaluation of the curative efficacy, the biocompatibility of the pure MTRNs was investigated (Fig. S8†). As cell survival rates approximate or even exceed 100% at the highest concentrations (1000 μg mL^{-1}), pure MTRNs show excellent biocompatibility. After that, antitumor efficiencies of CPT/MTRN were evaluated with MH (CPT/MTRN + MH) and without MH. Free CPT (low concentration of DMSO as the hydrotropy agent) and a culture

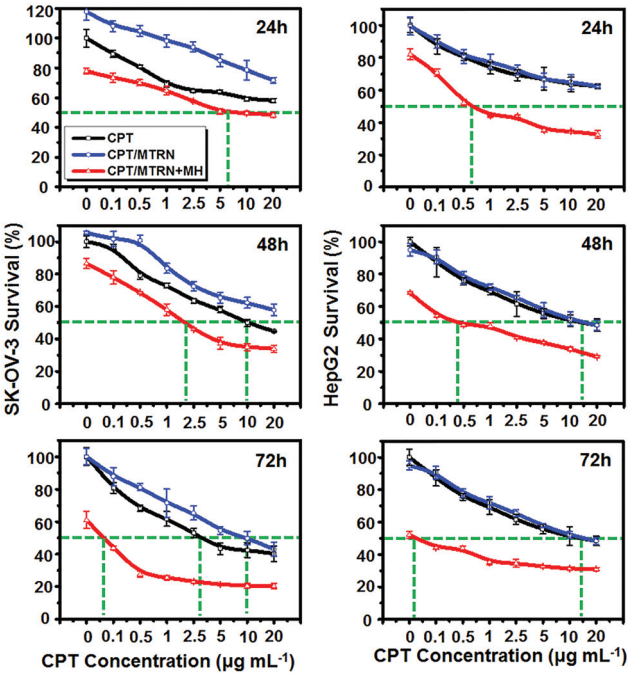

Fig. 2 The cytotoxicity of CPT under different treatments.

medium were used as positive and negative controls respectively.

As shown in Fig. 2, the CPT cytotoxicity is enhanced by periodic MH (5 min per 24 h). Viabilities of both types of cells were suppressed by CPT and CPT/MTRN, but by CPT/MTRN + MH more efficiently, for all tested periods. The gap of half maximal inhibitory concentration (IC_{50}) between the thermo-chemotherapy (CPT/MTRN + MH) and chemotherapy (CPT/MTRN or free CPT) is broadened with increasing time. As shown in Fig. 2, for SK-OV-3 at 72 h, IC_{50} of CPT/MTRN + MH is below 0.1 μg mL^{-1}, which is respectively less than 1/25 and 1/100 of its counterparts: free CPT and CPT/MTRN. For HepG2, IC_{50} of CPT/MTRN + MH is much lower than 0.1 μg mL^{-1} and much less than 1/100 of both chemotherapies at 72 h.

In addition to enhanced cytotoxicity of CPT, periodic MH suppresses cell viability, as evidenced in Fig. 2. As shown in Fig. 1c, CPT/MTRNs of high SAR (MZF of 100 μg mL^{-1}) can increase the surrounding temperature from 26 °C to 51.7 °C within 5 min under AMF (f = 114 kHz, $H_{applied}$ = 89.9 kA m^{-1}). However, the effectiveness of hyperthermia depends on thermal dose, which is the energy required for cell death at a given exposure time (t) and temperature (T).[30] As shown in Fig. 2, while CPT/MTRNs display excellent magnetocaloric effects, periodic MH has only suppressed cell proliferation by 20% at 24 h. It has even induced thermotolerance for SK-OV-3 at 48 h. Nonetheless, MH of 5 min is sufficient to trigger CPT release (Fig. 1d) for enhanced cytotoxicity at 24 h (Fig. 2).

As CPT was found undetectable by a flow cytometer (FCM), hydrophobic Nile Red (NR) was used as a dye model of NR/MTRN. The cellular uptake of NR was measured quantitatively

by FCM and qualitatively observed by confocal laser scanning microscopy (CLSM). Both types of cells were incubated with NR/MTRN (1 μg mL^{-1} of NR and 100 μg mL^{-1} of MZF), in which the NR/MTRN + MH group was treated under AMF for 5 min. The FCM and CLSM results reveal that the efficiency of cellular uptake can be enhanced by MH. For SK-OV-3, FCM result shows that the NR fluorescence intensities by NR/MTRN + MH are significantly higher than those by NR/MTRN at all time-points, as shown in Fig. 3a. Similar results are observed by CLSM, as shown in Fig. 3b. After a 5 min exposure to AMF, the dramatic increase of the NR fluorescence intensity (red) can be seen clearly at all time-points. Moreover, the NR fluorescence intensity of NR/MTRN + MH at 5 min is comparable with its counterpart NR/MTRN at 240 min. For HepG2, similar phenomena are observed again, as can be seen in Fig. 3c (FCM results) and Fig. 3d (CLSM results). By CLSM results, HepG2 shows a stronger cellular uptake on NR/MTRN than that of SK-OV-3; however, MH can enhance its NR internalization as well. Especially, the cellular uptake enhanced by MH takes place mainly during the initial period of 5 min, as shown in Fig. 3d, the distinction of NR fluorescence intensities between NR/MTRN + MH and NR/MTRN are more obvious at 5 min than those at other time-points (60 min and 240 min).

Based on Fig. 1f, the cumulative drug release is 7.3% at 240 min under the physiological conditions (37 °C, PBS), which is much lower than its counterpart by MH of 5 min (57.5%, Fig. 1e). Therefore, concentration of free NR in NR/MTRN + MH is expected to be much higher than that in NR/MTRN. However, the gaps between NR/MTRN + MH and NR/MTRN are similar at all time-points, as shown in Fig. 3. These phenomena suggest that the enhancement of the cellular uptake depends primarily on real-time MH but not on the concentration of free drug, as hyperthermia can increase fluidity of cell membranes.[30] However, the real-time MH can trigger drug release and improve endocytosis synchronously. It is hard to distinguish whether NR/MTRN or free NR is the main

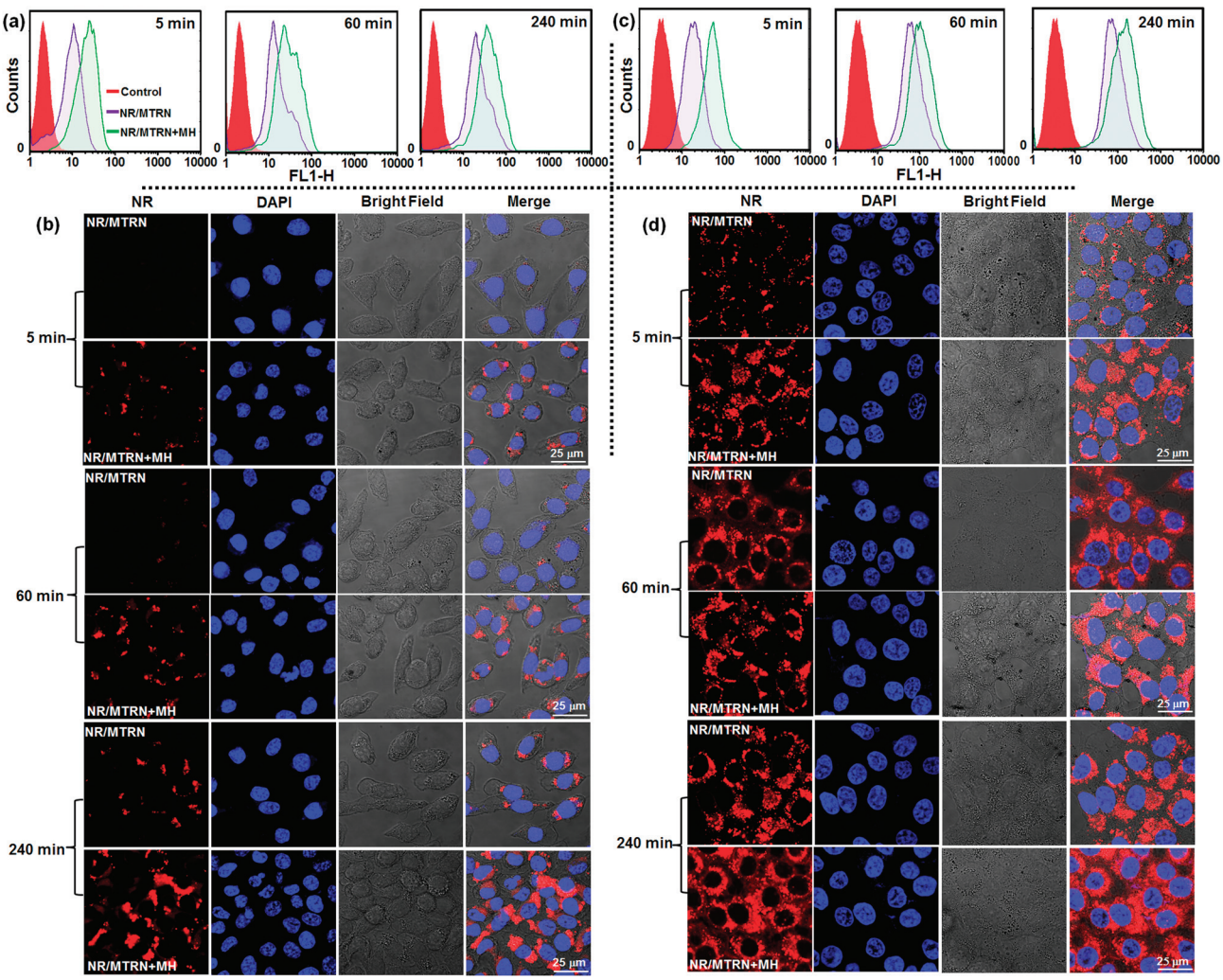

Fig. 3 The effect of efficient MH on the cellular uptake, characterized by FCM and CLSM: (a) FCM result of SK-OV-3, (b) CLSM results of SK-OV-3, (c) FCM result of HepG2, (d) CLSM results of HepG2.

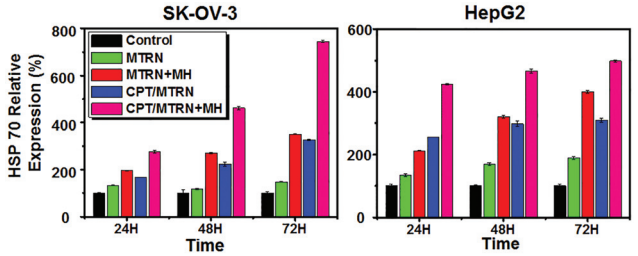

Fig. 4 HSP70 expression of SK-OV-3 and HepG2 under different treatments. Pure culture medium was used as a control.

source of enhanced NR fluorescence intensity in the cytoplasm. In spite of this, efficient MH has still shown its great advantage on the enhancement of cellular uptake in a short span of time. Consequently, MH can improve drug cytotoxicity by increasing its effective concentration, which contributes to the synergistic effect of MH and chemotherapy.

In addition to endocytosis, the key cellular response by hyperthermia is over-expression of HSPs, which is important for cellular protection against various stresses such as hyperthermia, infection, and poisoning.[30,40] Apparently, the expression of HSP70 can be up-regulated significantly by MH and chemotherapy alone. However, short-term MH (5 min per 24 h) is more effective on up-regulation of HSP70 expression than that of long-term CPT. The result indicates the potential of highly efficient MH on suppressing tumors, as evidenced in Fig. 2. Combing efficient MH with CPT, thermo-chemotherapy maximizes the up-regulation of HSP70 expression at all time-points, as shown in Fig. 4. Therefore, CPT/MTRN + MH can decrease IC_{50} of CPT significantly, compared to CPT alone (Fig. 2). In addition, the effect of MH and chemotherapy on HSP70 expression was found to depend on cell type. For SK-OV-3, MH was effective, with combined chemotherapy, to up-regulate expression of HSP70. Therefore, HSP70 expression and cell suppression of SK-OV-3 by CPT/MTRN + MH were found to increase in a similarly pronounced fashion. For HepG2, MH played a predominant role in HSP70 over-expression. As a result, suppression of HepG2 survival by MH was more efficient compared to SK-OV-3.

However, it is worth noting that a certain amount of HSP70 can protect cells from apoptosis by interacting with intracellular polypeptides and preventing their denaturation or incorrect assembly.[41] As a result, synergistic effect of efficient MH and high concentration CPT cannot reduce cell viability of SK-OV-3 and HepG2 further at 72 h, as can be seen in Fig. 2. In spite of that, HSP70 can also induce cell necrosis for its excess expression.[42] Necrotic cells can stimulate antitumor immune response to suppress the growth of tumor tissues by releasing abundant HSP70. Therefore, efficient thermo-chemotherapy shows another potential on immune activation, which benefits cancer immunotherapy.[43,44] HSP70 expression suggests that the balance between MH and chemotherapy is an important factor, which can be tailored in the design of the nanocarriers for efficient thermo-chemotherapy.

Conclusions

In summary, we have designed and developed highly synergistic MTRNs for efficient thermo-chemotherapy, and investigated their anti-tumor efficiency. By assembly of thermosensitive polymer, MNC and drug, the spherical MTRN exhibited the most effective synchronism of drug release and efficient MH. The synergistic effect of CPT and MH is achieved by enhanced CPT cytotoxicity. Furthermore, the operating mechanism is identified based on the enhanced cellular uptake by efficient MH and up-regulation of HSP70 expression by effective synchronism of thermo-chemotherapy. The experimental results show a clinically viable approach in tumor therapy by the synergetic effect of MH and chemotherapy.

Acknowledgements

This work was financially supported by the National High-Tech R&D Program of China (2013AA032202), the Science & Technology Commission of Shanghai Municipality (11nm0505100), the National Natural Science Foundation of China (51203118), and the Fundamental Research Funds for the Central Universities.

Notes and references

1 S. Laurent, S. Dutz, U. O. Häfeli and M. Mahmoudi, *Adv. Colloid Interface Sci.*, 2011, **166**, 8–23.
2 D. Ho, X. L. Sun and S. H. Sun, *Acc. Chem. Res.*, 2011, **44**, 875–882.
3 S. Behrens, *Nanoscale*, 2011, **3**, 877–892.
4 M. M. Yallapu, S. F. Othman, E. T. Curtis, B. K. Gupta, M. Jaggi and S. C. Chauhan, *Biomaterials*, 2011, **32**, 1890–1905.
5 K. Hayashi, M. Nakamura, W. Sakamoto, T. Yogo, H. Miki, S. Ozaki, M. Abe, T. Matsumoto and K. Ishimura, *Theranostics*, 2013, **3**, 366–376.
6 J. F. Berret, N. Schonbeck, F. Gazeau, D. E. Kharrat, O. Sandre, A. Vacher and M. Airiau, *J. Am. Chem. Soc.*, 2006, **128**, 1755–1761.
7 L. Lartigue, P. Hugounenq, D. Alloyeau, S. P. Clarke, M. Lévy, J. C. Bacri, R. Bazzi, D. F. Brougham, C. Wilhelm and F. Gazeau, *ACS Nano*, 2012, **6**, 10935–10949.
8 D. L. Shi, *Adv. Funct. Mater.*, 2009, **19**, 3356–3373.
9 T. S. Hauck, T. L. Jennings, T. Yatsenko, J. C. Kumaradas and W. C. W. Chan, *Adv. Mater.*, 2008, **20**, 3832–3838.
10 P. Schildkopf, O. J. Ott, B. Frey, M. Wadepohl, R. Sauer, R. Fietkau and U. S. Gaipl, *Curr. Med. Chem.*, 2010, **17**, 3045–3057.
11 R. D. Issels, *Eur. J. Cancer*, 2008, **44**, 2546–2554.
12 H. Oliveira, E. Pérez-Andrés, J. Thevenot, O. Sandre, E. Berra and S. Lecommandoux, *J. Controlled Release*, 2013, **169**, 165–170.

13 L. A. Tziveleka, P. Bilalis, A. Chatzipavlidis, N. Boukos and G. Kordas, *Macromol. Biosci.*, 2014, **14**, 131–141.

14 P. M. Peiris, L. Bauer, R. Toy, E. Tran, J. Pansky, E. Doolittle, E. Schmidt, E. Hayden, A. Mayer, R. A. Keri, M. A. Griswold and E. Karathanasis, *ACS Nano*, 2012, **6**, 4157–1468.

15 V. Plassat, C. Wilhelm, V. Marsaud, C. Ménager, F. Gazeau, J. Renoir and S. Lesieur, *Adv. Funct. Mater.*, 2011, **21**, 83–92.

16 W. L. Chiang, C. J. Ke, Z. X. Liao, S. Y. Chen, F. R. Chen, C. Y. Tsai, Y. N. Xia and H. W. Sung, *Small*, 2012, **8**, 3584–3588.

17 S. H. Hu, B. J. Liao, C. S. Chiang, P. J. Chen, I. W. Chen and S. Y. Chen, *Adv. Mater.*, 2012, **24**, 3627–3632.

18 R. Chandrawati, P. D. Odermatt, S. F. Chong, A. D. Price, B. Stadler and F. Caruso, *Nano Lett.*, 2011, **11**, 4958–4963.

19 D. Kim, G. G. Zhong, E. S. Lee and H. B. You, *Mol. Pharm.*, 2009, **6**, 1353–1362.

20 K. Kono, T. Ozawa, T. Yoshida, F. Ozaki, Y. Ishizaka, K. Maruyama, C. Kojima, A. Harada and S. Aoshima, *Biomaterials*, 2010, **31**, 7096–7105.

21 A. Agarwal, M. A. Mackey, M. A. El-Sayed and R. V. Bellamkonda, *ACS Nano*, 2011, **5**, 4919–4926.

22 X. Ding, K. Cai, Z. Luo, J. Li, Y. Hu and X. Shen, *Nanoscale*, 2012, **4**, 6289–6292.

23 S. Purushotham and R. V. Ramanujan, *Acta Biomater.*, 2010, **6**, 502–510.

24 S. R. Deka, A. Quarta, R. D. Corato, A. Riedinger, R. Cingolania and T. Pellegrino, *Nanoscale*, 2011, **3**, 619–629.

25 T. Todd, Z. Zhen, W. Tang, H. Chen, G. Wang, Y-J. Chuang, K. Deaton, Z. Pan and J. Xie, *Nanoscale*, 2014, **6**, 2073–2076.

26 K. Cheng, S. Peng, C. J. Xu and S. H. Sun, *J. Am. Chem. Soc.*, 2009, **131**, 10637–10644.

27 L. Y. Qu, J. Ren, W. Yuan and D. Shi, *Nanotechnology*, 2012, **23**, 505706.

28 M. Zheng, C. Yue, Y. Ma, P. Gong, P. Zhao, C. Zheng, Z. Sheng, P. Zhang, Z. Wang and L. Cai, *ACS Nano*, 2013, **7**, 2056–2067.

29 J. Park, G. Maltzahn, L. L. Ong, A. Centrone, T. A. Hatton, E. Ruoslahti, S. N. Bhatia and M. J. Sailor, *Adv. Mater.*, 2010, **22**, 880–885.

30 H. P. Wust, O. Ahlers, A. Dieing, G. Sreenivasa, T. Kerner, R. Felix and H. Riess, *Crit. Rev. Oncol./Hemat.*, 2002, **43**, 33–56.

31 J. O. W. Pelz, M. Vetterlein, T. Grimmig, A. G. Kerscher, E. Moll, M. Lazariotou, N. Matthes, M. Faber, C. T. Germer, A. M. Waaga-Gasser and M. Gasser, *Ann. Surg. Oncol.*, 2013, **20**, 1105–1113.

32 S. H. Sun, H. Zeng, D. B. Robinson, S. Raoux, P. M. Rice, S. X. Wang and G. Li, *J. Am. Chem. Soc.*, 2004, **126**, 273–279.

33 X. Liu, H. M. Fan, J. B. Yi, Y. Yang, E. S. G. Choo, J. M. Xue, D. D. Fan and J. Ding, *J. Mater. Chem.*, 2012, **22**, 8235–8244.

34 S. Brulé, M. Levy, C. Wilhelm, D. Letourneur, F. Gazeau, C. Ménager and C. L. Visage, *Adv. Mater.*, 2011, **23**, 787–790.

35 R. Hao, J. Yu, Z. Ge, L. Zhao, F. Sheng, L. Xu, G. Li and Y. Hou, *Nanoscale*, 2013, **5**, 11954–11963.

36 I. C. Rubio, M. Insausti, E. Garayo, I. G. de Muro, F. Plazaola, T. Rojo and L. Lezama, *Nanoscale*, 2014, **6**, 7542–7552.

37 J. Jang, H. Nah, J. Lee, S. H. Moon, M. G. Kim and J. Cheon, *Angew. Chem., Int. Ed.*, 2009, **121**, 1260–1264.

38 J. Liu, C. Detrembleur, A. Debuigne, M. Pauw-Gillet, S. Mornet, L. V. Elst, S. Laurent, C. Labrug`ere, E. Duguet and C. Jérôme, *Nanoscale*, 2013, **5**, 11464–11477.

39 E. Peng, E. S. G. Choo, P. Chandrasekharan, C.-T. Yan, J. Ding, K. H. Chuang and J. M. Xue, *Small*, 2012, **8**, 3620–3630.

40 V. Milani, E. Noessner, S. Ghose, M. Kuppner, B. Ahrens, A. Scharner, R. Gastpar and R. D. Issels, *Int. J. Hyperthermia*, 2002, **18**, 563–575.

41 K. A. Buzzard, A. J. Giaccia, M. Killender and R. L. Anderson, *J. Biol. Chem.*, 1998, **273**, 17147–17153.

42 S. Yokota and N. Fujii, *Microbiol. Immunol.*, 2010, **54**, 299–307.

43 B. Frey, E. M. Weiss, Y. Rubner, R. Wunderlich, O. J. Ott, R. Sauer, R. Fietkau and U. S. Gaipl, *Int. J. Hyperthermia*, 2012, **28**, 528–542.

44 A. Ito, H. Honda and T. Kobayashi, *Cancer Immunol. Immunother.*, 2006, **55**, 320–328.